THE JOURNAL OF PHYSICAL CHEMISTRY C

ARTICLE

pubs.acs.org/JPCC

Facile Synthesis and Photocatalysis of Size-Distributed TiO_2 Hollow Spheres Consisting of {116} Plane-Oriented Nanocrystallites

Yuzhu Jiao,[‡] Chengxin Peng,[†] Fangfang Guo,[†] Zhihao Bao,[†] Jinhu Yang,[*,†,§] Lukas Schmidt-Mende,[§] Ricky Dunbar,[§] Yao Qin,[*,†] and Zifeng Deng[‡]

[†]Institute for Advanced Materials and Nano Biomedicine and [‡]Department of Chemistry, Tongji University, Siping Road 1239, Shanghai 200092, People's Republic of China

[§]Department of Physics and Center for Nanoscience (CeNS), Ludwig-Miximilians University, Amalienstr. 54, D-80799 Munich, Germany

Supporting Information

ABSTRACT: TiO_2 hollow spheres consisting of highly active {116} plane-oriented crystallites have been synthesized with a wide diameter distribution from 20 nm to over 5 μm via a facile emulsion method. The prepared hollow spheres possess large specific surface area (S_{BET} = 104 m^2/g) and mesopores (15.7 nm), which could be further modified by Pt doping. The mechanisms for hollow sphere formation and {116} plane orientation are discussed briefly. Moreover, compared with normal TiO_2 hollow spheres, which usually exhibit uniform diameter distributions and no specific plane orientation, the typical TiO_2 hollow spheres with and without Pt doping exhibit good photocatalytic activities for phenol degradation under visible and UV light irradiation. The wide diameter (i.e., curvature) distribution, high specific surface area, conduciveness to forming mesoporous structures, and exposed high-energy surfaces allow good molecular infiltration and adsorption as well as photoelectroactivity and make them attractive for light harvesting.

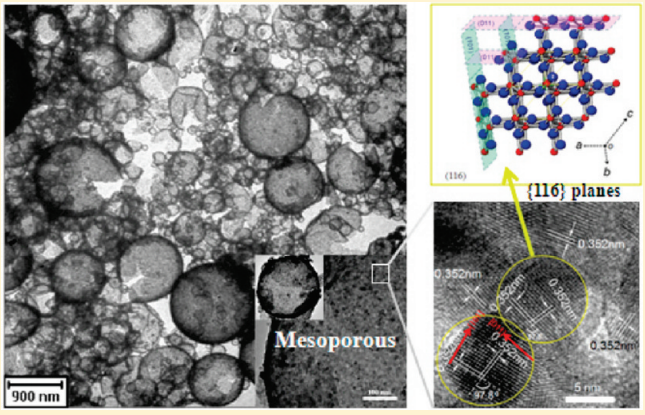

INTRODUCTION

TiO_2 hollow spheres have attracted considerable attention because of their low density, high specific surface area, and high mobility, which promise applications in various areas, such as light-trapping, chemical separation, photocatalysis, photovoltaics, and optical devices.[1,2] The methods for TiO_2 hollow sphere preparation have been well developed, such as the spray-drying technique,[3] Ostwald-ripening[4] or analogous hollowing processes induced by F^- ions,[5] and templating methods involving hard colloidal spheres[6−10] or soft emulsion droplets.[11−13] Among these, the soft emulsion method offers high versatility. It is often performed at low temperature and no additional effort is necessary for template removal. However, there are only limited successes toward TiO_2 hollow sphere preparation by emulsion templating,[12,13] owing possibly to the comlexity of soft emulsion system with flexiable shapes for dynamically directing Ti-precursor hydrolysis. Besides, TiO_2 hollow spheres obtained so far by this method are mainly uniform or narrowly distributed in diameter, which would confine their specific properties toward applications. In this paper, we developed a facile emulsion route based on octadecene/formamide for one-pot synthesis of TiO_2 hollow spheres with a wide diameter distribution from nano- to microscale and, in paricular, shells consisting of highly {116} facet-oriented crystallites after heat treatment.

It is noteworthy that hollow spheres with curved surfaces could multireflect incident light by inner walls of shells and thus increase light-harvesting efficiency in photocatalysis or solar cells.[1,14−16] Moreover, hollow spheres with different sizes can respectively respond to light of different wavelengths.[16−18] Hence, TiO_2 hollow spheres prepared with diameters ranging widely from nano- to microscale would have increased reflection in a wide band of incident light, which is beneficial for enhanced light capturing. As a catalyst, the photoelectric activity of TiO_2 depends highly not only on its particle size and shape, but also on crystal facets/planes exposed because different planes may have different surface energies. As documented, TiO_2 facets with higher surface energies are more active in catalytic reactions. Facets with {001} and {110} orientation show better photocatalytic activity than lower surface energy {101} facets.[19−21] Moreover, higher-energy facets present weaker or even negligible signals in XRD patterns because they are

Received: January 17, 2011
Revised: March 3, 2011
Published: March 18, 2011

energy-unstable and only exist if stabilized under specific conditions. For instance, surface energies of {101}, {100}, {001}, {103}, and {110} planes increase from 0.44, 0.53, 0.90, and 0.93 to 1.09 J m^{-2}, respectively,[22] while their corresponding peaks in XRD pattern decrease from 100% to 6%. In the standard XRD pattern of anatase TiO_2, the diffraction peak of {116} planes has 6% intensity, similar to that of {110} planes. Accordingly, {116} planes should have similar surface energy as {110} planes and theoretically higher photoelectric activity than the other planes mentioned above. Therefore, TiO_2 hollow spheres with wide diameter distribution and highly active {116} plane orientation are expected to be promising candidates for a wide range of applications.

EXPERIMENTAL SECTION

Preparation of TiO_2 Hollow Spheres. In a typical synthesis of TiO_2 hollow spheres, 4.43 mL of formamide containing 0.13 g of sodium dodecyl sulfate and 0.46 mL of octadecene containing 0.142 g titanium butoxide were mixed and sonicated for 1 min and then 2.2 mL of formamide containing 0.03 g of H_2O was added with stirring. Here formamide and octadecene served as water phase and oil phase, while H_2O was used for titanium butoxide hydrolysis, respectively. Subsequently, the mixed solution was kept in a water bath at 30 °C for 45 min, giving a white supernatant product. The product was collected after centrifugation, washed with water, and then put into an oven at 480 °C for 3 h for crystallization.

Pt Doping of TiO_2 Hollow Spheres. A 0.5 g portion of TiO_2 hollow spheres prepared from the emulsion method was dispersed into 10 mL of H_2PtCl_6 (1×10^{-2} M) under stirring for 20 h and then collected after centrifugation and redispersed into 5 mL of H_2O. Subsequently, 5 mL of 10 mg/L $NaBH_4$ was added as reductant with stirring, resulting in Pt deposition on TiO_2 hollow spheres. The Pt-doped TiO_2 hollow spheres were washed repeatedly, collected, and dried in an oven at 60 °C. The Pt existence was confirmed by XRD and EDX characterizations.

Characterizations. The TiO_2 hollow sphere samples were characterized by scanning electron microscopy (SEM, AMARY 1910, 10 kV), high-resolution transmission electron microscopy (HR-TEM, JEOL 2011, 200 kV) combined with an energy dispersed X-ray analyzer, and powder X-ray diffraction (XRD) using a D/max2550VB3+/PC X-ray diffractometer with Cu Ka radiation with a 1.5418 Å wavelength. A beam voltage of 40 kV and a 100 mA current beam were used. The Brunauer–Emmett–Teller (BET) specific surface area (S_{BET}) of the powders was analyzed by nitrogen adsorption in a Tristar 3000 nitrogen adsorption apparatus.

The Photocatalytic Activity Evaluation. The photocatatic activities of TiO_2 hollow spheres without and with Pt doping were evaluated in terms of phenol degradation under ultraviolet (UV) and visible light by using a Xe lamp (254 nm) and UV light filter (wavelength <440 nm was filtered out), respectively. Briefly, 0.02 g of TiO_2 hollow spheres or Pt-doped TiO_2 was dispersed into 30 mL of 2.1×10^{-4} M phenol solution. Before irradiation, the suspension was stirred for 30 min to ensure maximal adsorption of phenol molecules on catalysts. Then the suspension was irradiated under light and sampled at a given time interval (10 min for TiO_2 hollow spheres and 1 h for Pt-doped TiO_2 hollow spheres). The specimens were centrifuged and measured by UV–vis spectrometer (Varian Cary 500) to determine residual phenol.

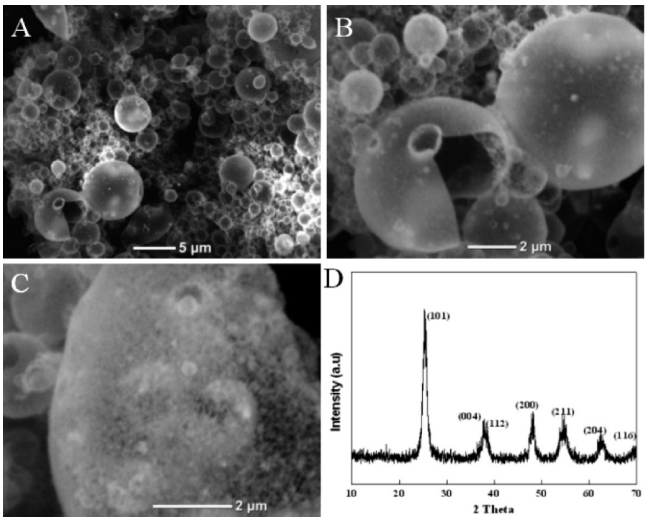

Figure 1. SEM images (A–C) and XRD pattern (D) of TiO_2 hollow spheres with a wide size distribution.

RESULTS AND DISCUSSION

Typical TiO_2 hollow spheres synthesized at large scale are presented in Figure 1. It is shown clearly that as-prepared TiO_2 spheres have smooth surfaces and a wide diameter distribution, estimated to range from 50 nm to over 5 μm (Figure 1A,B). The low image contrast and, particularly, some broken spheres with thin shells both display the hollow interior of these TiO_2 spheres. A magnified scanning electron microscopy (SEM) image of a broken TiO_2 hollow sphere with smaller spheres attached to its surface is shown in Figure 1C, showing a thin shell consisting of dense and uniform crystallites. Similar to interfacial reactions in ionic liquids,[11] we also think that the hollow structure of TiO_2 is formed through a mechanism involving a diffusion process of Ti-OR groups from inner core to interfaces of emulsions and then a hydrolysis process on interfaces with trace amounts of water, as illustrated in Figure S1 (Supporting Information). TiO_2 hollow spheres are well-crystallized after annealing, and the crystallites as building units of the smooth shells are estimated to be at nanometer scale, which are evident from the intensified and widened peaks of the X-ray diffraction (XRD) pattern (JCPDS card no. 21-1272; a, b = 3.78 Å; c = 9.51 Å; $\alpha = \beta = \gamma = 90°$) in Figure 1D.

More detailed structural information of TiO_2 hollow spheres is given in Figure 2. An overviewed TEM image reveals an interior enclosed by a thin shell of TiO_2 (Figure 2A). In addition, different diameters of the TiO_2 hollow spheres ranging widely from nano- to microscale are observed (see also Figure S2, Supporting Information, for statistical analysis of TiO_2 diameter distribution). Furthermore, an individual hollow sphere was selected arbitrarily to give closer characterization (inset of Figure 2B). An enlarged TEM image in Figure 2B indicates that the shell thickness is only ~10 nm and consists of large numbers of crystallites (5–10 nm) with lots of intercrystallite nanopores uniformly dispersed (Figure 2B), revealing a mesoporous structure with a large surface area. The detailed data of average pore diameter and specific surface area (S_{BET}) of hollow spheres were measured to be 15.7 nm and 104.7 m^2/g, respectively (Figure 3), where specific surface area is higher than that of commercial Degussa P25 (P25) powder (49.5 m^2/g) and previously reported TiO_2 hollow spheres (56–77 m^2/g).[5,15,23] At a high resolution,

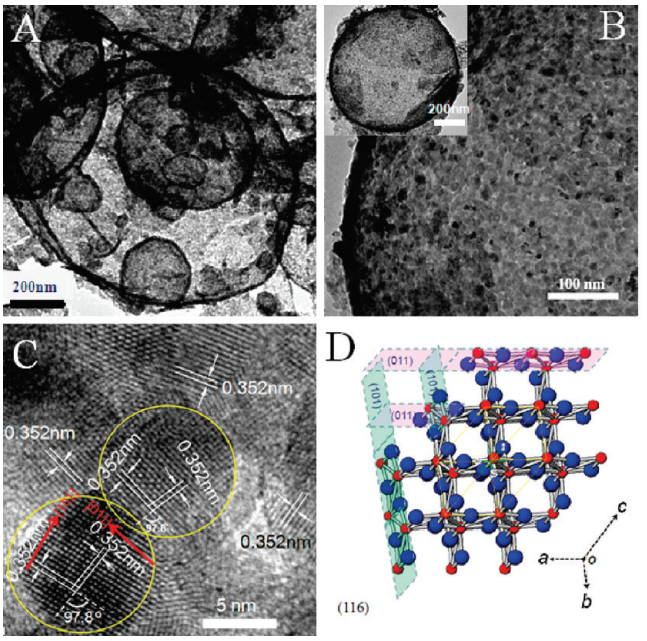

Figure 2. TEM (A, B) and HRTEM (C) images of TiO_2 hollow spheres, and (D) the crystal structure diagram along TiO_2 {116} planes. The inset in panel B is a hollow sphere arbitrarily selected for local sited HRTEM. Red spheres and blue spheres in D present Ti atoms and O atoms, respectively.

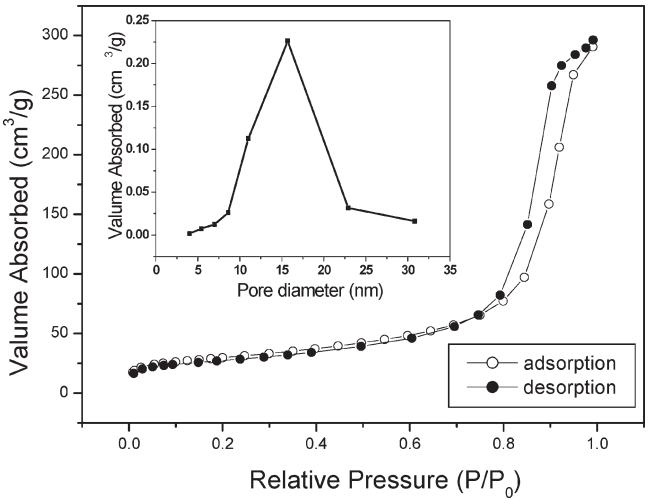

Figure 3. Nitrogen adsorption−desorption isotherm of the TiO_2 hollow spheres. The inset shows the corresponding pore size distribution obtained from the adsorption curve.

clear boundaries and crystal lattice fringes of crystallites with diameters of 5−10 nm were observed. A set of crystal lattices with *d*-space equivalent to 0.352 nm corresponding to {101} planes of anatase TiO_2 is found as the majority faces of individual crystallites throughout the area observed (Figures 2C and S3, Supporting Information). For each individual crystallite, such fringes with the exact *d*-spacing that appeared in pairs show an included angle of 97.8° (see areas labeled with circles in Figure 2C), identifying {101} planes as side faces and {116} planes as top faces (see Supporting Information for calculation). For a more intuitive understanding of {116} orientation, the crystal structure of {116} planes

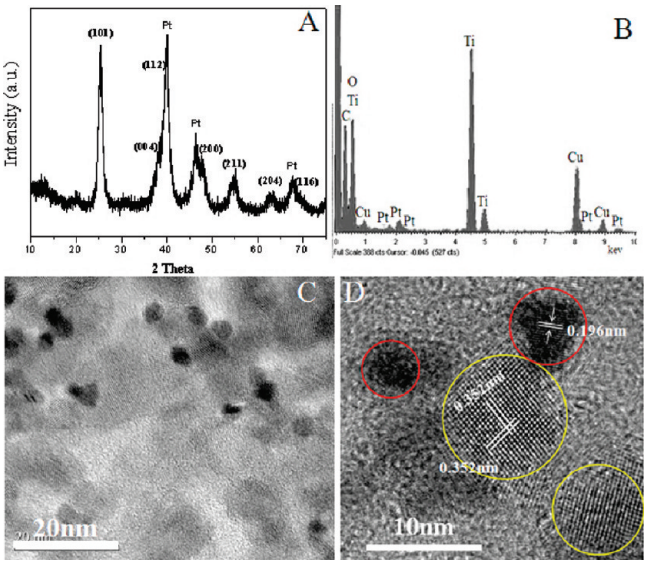

Figure 4. XRD and EDX patterns and high-resolution TEM images of TiO_2 hollow spheres with Pt doping.

viewed from their normal line, i.e. the $[11\bar{1}]$ direction, is illustrated in Figure 2D. Here, the {116} planes lay horizontally as the top face while two equivalent planes of {101} and {011} stand vertically as the side faces with an angle of 97.8°, which is in accordance with crystal lattice data observed in Figure 2C. The orientation of {116} planes achieved here for the first time is interesting because it was realized by simply annealing amorphous hollow spheres without any additives.

The mechanism that favors this crystal plane orientation of crystallites relies possibly on two factors: (1) spatial proximity and (2) energy feasibility. Regarding spatial proximity, the uniform and thin shell thickness (∼10 nm) of shells of amorphous hollow spheres provides confined space for crystal nucleus partners to recognize each other during the annealing and crystallization process, which avoids the adversity of long-distance diffusion of solid reactions and enables free rotation and recognization through {101} planes of the crystallites to form {116} plane orientation. Considering energy feasibility, although {116} planes of TiO_2 crystallites are relatively unstable and active in energy, the intercrystallite recognition or aggregation of crystallites along energy-stable {101} planes is thermodynamically favorable, which directs the general crystallization processes to proceed in an energy-minimizing pathway under this condition.

The TiO_2 hollow spheres were further modified with Pt doping. As shown in Figure 4A, the XRD pattern of TiO_2 hollow spheres after Pt doping displays a set of sharp and widened peaks, in addition to those of anatase TiO_2, which can be assigned to the cubic structure of Pt (JCPDS card no. 04-0802), indicating that the TiO_2 shells were successfully decorated with well-crystallized Pt nanoparticles. The Pt existence in TiO_2 hollow sphere sample was also evidenced by the EDX pattern showed in Figure 4 B. From TEM images in Figure 4 C,D, it can be seen that Pt nanoparticles (in black contrast) have an average size of 2−3 nm and disperse discretely on TiO_2 shell. A Pt nanoparticle (in red circle) shows a set of lattice frings with *d*-spacing equivalent to 0.196 nm, corresponding to {200} planes, confirming a pure platinum phase of the nanoparticles. In addition, the {116} plane orientation was found to be still preserved for TiO_2 crystallites after Pt doping, which is highlightened by the yellow circles in Figure 4D.

dx.doi.org/10.1021/jp200491u |*J. Phys. Chem. C* 2011, 115, 6405–6409

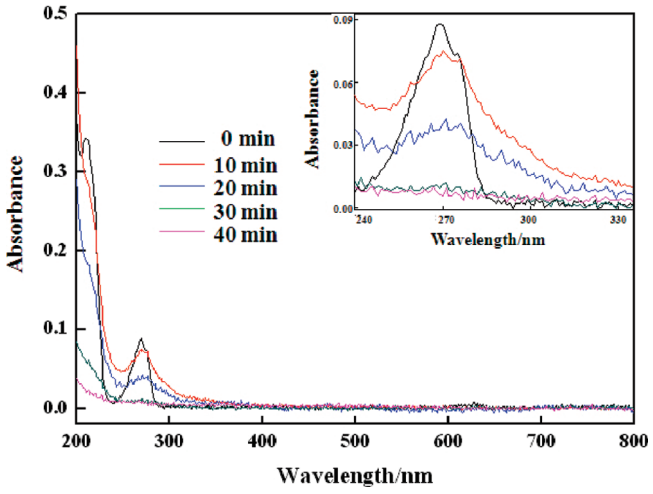

Figure 5. Example of phenol degradation data with time under UV irradiation with 0.66 g/L TiO_2 hollow spheres in 2.1 × 10^{-4} M phenol solution. The inset is an enlarged part of the diagram where the waveband of phenol peaks intensify.

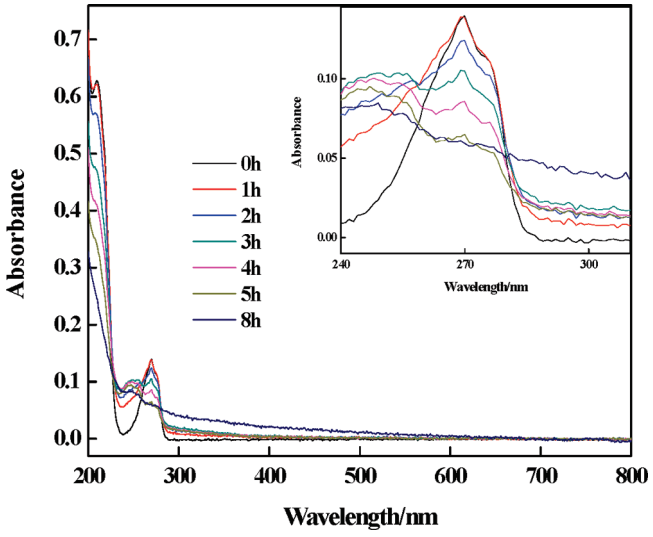

Figure 6. Example of phenol degradation data with time under visible light irradiation at a concentration of 0.66 g/L TiO_2 hollow spheres in 2.1 × 10^{-4} M phenol solution. The inset is an enlarged part of the diagram where the waveband of phenol peaks intensify.

The as-synthesized TiO_2 hollow spheres with the specific characteristics of wide size distribution and oriented {116} planes were further applied to the photocatalytic reaction of phenol degradation. Phenol degradation was used as a model process to investigate the effect of diameter distribution and plane orientation on the photocatalytic activity of TiO_2 hollow spheres. The hollow spheres with the above-described synthesis were compared with hollow spheres (see Supporting Information) that exhibited a narrow diameter distribution centered at 450 nm and no preferred crystallographic orientation (Supporting Information, Figure S4). It was found that under UV light irradiation, phenol with a concentration of 2.1 × 10^{-4} M was degraded completely within 30 min in the presence of 0.66 mg/L typical TiO_2 hollow spheres (Figure 5) and around 50 min for normal TiO_2 hollow spheres with uniform diameter at the same concentration (Supporting Information, Figure S5). The photocatalytic activity is almost twice of the size distributed TiO_2 hollow spheres compared with 450 nm hollow spheres. Photocatalysis of phenol degradation in the presence of Pt-doped TiO_2 hollow spheres was also conducted, as illustrated in Figure 6. Under visible light, phenol of same concentration (2 × 10^{-4} M) could be degraded completely within 5 h. Both types of TiO_2 hollow spheres with and without Pt doping exhibit good photocatalytic activities. Considering direct light scattering by big hollow spheres with sizes over 5 μm, which will decrease efficient light harvesting of the catalyst, the photocatalytical performance could possibly be further improved by simply filtering big hollow spheres out. It is noteworthy that the maximum adsorption capacity of phenol on size-distributed TiO_2 hollow spheres was examined to be 1.8 mg/L (Supporting Information, Figure S6), indicating a poor static adsorption ability of the pure TiO_2 hollow spheres, though having a large surface area. However, the static adsorption capacity is not a key factor to determine the dynamic process of photocatalysis. For this phenol photodegradation, the dynamic diffusion and adsorption and desorption of phenol molecules, as well as highly active TiO_2 {116} planes, may play more key roles than the static adsorption in the catalytic reactions proceeding, which contributed to the good performance.

CONCLUSION

In conclusion, TiO_2 hollow spheres with wide diameter distribution have been prepared via a facile emulsion method. Moreover, the as-prepared hollow spheres have highly uniform shells, possess large specific surface area (S_{BET} = 104 m^2/g), mesopores (15.7 nm), and especially highly active {116} plane-oriented crystallites. These are advantageous to related photoelectric applications due to advantages in light-harvesting and molecule adsorption and transport, as well as large and active surface area. The TiO_2 hollow spheres with and without Pt doping exhibit good photocatalytic activities for phenol degradation under visible and UV light irradiation, respectively. It can be expected that the hollow spheres will also be employed in other applications, such as sensors, photoelectric devices, and photovoltaic cells, leading to improved performance.

ASSOCIATED CONTENT

Supporting Information. Experimental procedure for synthesis of TiO_2 hollow sphere by PS templating, calculations of {116} planes, and Figures S1−S6. This material is available free of charge via the Internet at http://pubs.acs.org.

AUTHOR INFORMATION

Corresponding Author

*E-mail: yangjinhu2010@gmail.com (J.Y.), qinyao83@gmail.com (Y.Q.). Tel: +86-21-65988029. Fax: +86-21-65983706.

ACKNOWLEDGMENT

Thanks for financial support from National Natural Science Foundation (21001082), Shanghai Pujiang Program (10PJ1410400), Research Fund for the Doctoral Program of Higher Education of China (20090072120013), Program for New Century Excellent Talent in University (No. NCET-10-0595), the Program for Young Excellent Talents in Tongji University

(2008KJ046, 2009KJ075, and 2009KJ076), and Alexander von Humboldt Foundation for a Fellowship.

REFERENCES

(1) Pan, J. H.; Zhang, X. W.; Du, A. J.; Sun, D. D.; Leckie, J. O. *J. Am. Chem. Soc.* **2008**, *130*, 11256–11257.
(2) Koo, H. J.; Kim, Y. J.; Lee, Y. H.; Lee, W. I.; Kim, K.; Park, N. G. *Adv. Mater.* **2008**, *20*, 195–199.
(3) Iida, M.; Sasaki, T.; Watanabe, M. *Chem. Mater.* **1998**, *10*, 3780–3782.
(4) (a) Yang, H. G.; Zeng, H. C. *J. Phys. Chem. B* **2004**, *108*, 3492–3495. (b) Li, J.; Zeng, H. C. *Angew. Chem., Int. Ed.* **2005**, *44*, 4342–4345.
(5) Yu, J. G.; Zhang, J. *Dalton Trans.* **2010**, *39*, 5860–5867.
(6) Caruso, F.; Shi, X.; Caruso, R. A.; Susha, A. *Adv. Mater.* **2001**, *13*, 740–744.
(7) Caruso, R. A.; Susha, A.; Caruso, F. *Chem. Mater.* **2001**, *13*, 400–409.
(8) Wang, L.; Sasaki, T.; Ebina, Y.; Kurashima, K.; Watanabe, M. *Chem. Mater.* **2002**, *14*, 4827–4832.
(9) Li, G. Q.; Liu, C. Y.; Liu, Y. *J. Am. Ceram. Soc.* **2007**, *90*, 2667–2669.
(10) Xuan, S. H.; Jiang, W. Q.; Gong, X. L.; Hu, Y.; Chen, Z. Y. *J. Phys. Chem. C* **2009**, *113*, 553–558.
(11) Takuya, N.; Nobuo, K. *J. Am. Chem. Soc.* **2003**, *125*, 638–639.
(12) Collins, A. M.; Spickermann, C.; Mann, S. *J. Mater. Chem.* **2003**, *13*, 1112–1114.
(13) Eun, T. H.; Kom, S.-H.; Jeong, W.-J.; Jeon, S.-J.; Kim, S.-H.; Yang, S.-M. *Chem. Mater.* **2009**, *21*, 201–203.
(14) Qian, J. F.; Liu, P.; Xiao, Y.; Jiang, Y.; Cao, Y.; Ai, X. P.; Yang, H. X. *Adv. Mater.* **2009**, *21*, 3663–3667.
(15) Kondo, Y.; Yoshikawa, H.; Awaga, K.; Murayama, M.; Mori, T.; Sunada, K.; Bandow, S.; Iijima, S. *Langmuir* **2008**, *24*, 547–550.
(16) Li, H.; Bian, Z.; Zhu, J.; Zhang, D.; Li, G.; Huo, Y.; Li, H.; Lu, Y. *J. Am. Chem. Soc.* **2007**, *129*, 8406–8407.
(17) Ferber, J.; Luther, J. *Sol. Energy Mater. Sol. Cells* **1998**, *54*, 265–275.
(18) Kim, S. H.; Cho, Y. S.; Jeon, S. J.; Eun, T. H.; Yi, G. R.; Yang, S. M. *Adv. Mater.* **2008**, *20*, 3268–3273.
(19) Gong, X. Q.; Selloni, A. *J. Phys. Chem. B* **2005**, *109*, 19560–19562.
(20) (a) Yang, H. G.; Sun, C. H.; Qiao, S. Z.; Zou, J.; Liu, G.; Smith, S. C.; Cheng, H. M.; Lu, G. Q. *Nature* **2008**, *453*, 638–641. (b) Yang, H. G.; Liu, G.; Qiao, S. Z.; Sun, C. H.; Jin, Y. G.; Smith, S. C.; Zou, J.; Cheng, H. M.; Lu, G. Q. *J. Am. Chem. Soc.* **2009**, *131*, 4078–4083.
(21) Liu, M.; Piao, L. Y.; Zhao, L.; Ju, S. T.; Yan, Z. J.; He, T.; Zhou, C. L.; Wang, W. J. *Chem. Commun.* **2010**, *46*, 1664–1666.
(22) Lazzeri, M.; Vittadini, A.; Selloni, A. *Phys. Rev. B: Condens. Matter Mater. Phys.* **2002**, *65*, 119901.
(23) Kowalska, E.; Remita, H.; Colbeau-Justin, C.; Hupka, J.; Belloni, J. *J. Phys. Chem. C* **2008**, *112*, 1124–1131.